Since January 2020 Elsevier has created a COVID-19 resource centre with free information in English and Mandarin on the novel coronavirus COVID-19. The COVID-19 resource centre is hosted on Elsevier Connect, the company's public news and information website.

Antiviral Research 197 (2022) 105232

Contents lists available at ScienceDirect

Antiviral Research

journal homepage: www.elsevier.com/locate/antiviral

S-adenosylmethionine-dependent methyltransferase inhibitor DZNep blocks transcription and translation of SARS-CoV-2 genome with a low tendency to select for drug-resistant viral variants

Ram Kumar, Nitin Khandelwal, Yogesh Chander, Himanshu Nagori, Assim Verma, Aditya Barua, Bhagraj Godara, Yash Pal, Baldev R. Gulati, Bhupendra N. Tripathi [***,1], Sanjay Barua [**], Naveen Kumar [*]

National Centre for Veterinary Type Cultures, ICAR-National Research Centre on Equines, Hisar, India

ARTICLE INFO

Keywords:
DZNep
Epitranscriptomic
SARS-CoV-2
Virus replication
Drug resistance

ABSTRACT

We report the *in vitro* antiviral activity of DZNep (3-Deazaneplanocin A; an inhibitor of S-adenosylmethionine-dependent methyltransferase) against SARS-CoV-2, besides demonstrating its protective efficacy against lethal infection of infectious bronchitis virus (IBV, a member of the *Coronaviridae* family). DZNep treatment resulted in reduced synthesis of SARS-CoV-2 RNA and proteins without affecting other steps of viral life cycle. We demonstrated that deposition of N6-methyl adenosine (m6A) in SARS-CoV-2 RNA in the infected cells recruits heterogeneous nuclear ribonucleoprotein A1 (hnRNPA1), an RNA binding protein which serves as a m6A reader. DZNep inhibited the recruitment of hnRNPA1 at m6A-modified SARS-CoV-2 RNA which eventually suppressed the synthesis of the viral genome. In addition, m6A-marked RNA and hnRNPA1 interaction was also shown to regulate early translation to replication switch of SARS-CoV-2 genome. Furthermore, abrogation of methylation by DZNep also resulted in defective synthesis of the 5' cap of viral RNA, thereby resulting in its failure to interact with eIF4E (a cap-binding protein), eventually leading to a decreased synthesis of viral proteins. Most importantly, DZNep-resistant mutants could not be observed upon long-term sequential passage of SARS-CoV-2 in cell culture. In summary, we report the novel role of methylation in the life cycle of SARS-CoV-2 and propose that targeting the methylome using DZNep could be of significant therapeutic value against SARS-CoV-2 infection.

1. Introduction

Gene expression is not determined solely by the sequence information encoded in the individual's genome but is rather subjected to multiple levels of control both at the DNA and RNA levels. At the DNA (genomic) level, besides promoters and enhancers, the gene expression is regulated by DNA methylation, histone remodelling, alternative histone variant use and deposition of modifications on histone tails, collectively referred to as epigenetic regulation (Chokkalla et al., 2020). Similarly, covalent modifications also contribute in determining the stability and translation of mRNA and are referred to as epitranscriptomic gene regulation (Seo and Kleiner, 2021). Out of the over 160 different posttranscriptional modifications described so far, most are abundantly present in ribosomal RNA (rRNA) and transfer RNA (tRNA) (Boccaletto and Baginski, 2021). The messenger RNA (mRNA) also contains at least 13 different chemical modifications (Anreiter et al., 2021) which are grouped as cap-adjacent- and internal modifications (Anreiter et al., 2021). Internal modifications occur in coding regions, introns as well as 5′ and 3′ untranslated regions (UTRs) of mRNAs. The N^6-methyladenosine (m6A) is the most abundant internal modification of mRNA and long noncoding RNA (lncRNA) in mammalian cells (Anreiter et al., 2021). The enzymes that install, remove and bind to mRNA modifications are called as "writers" "erasers" and "readers" respectively. m6A is installed by a methyltransferase complex (writers) containing the core catalytic heterodimer [methyltranferase-like protein 3 (METTL3) and METTL14] and a splicing factor WTAP (Wilms tumor

* Corresponding author.
** Corresponding author.
*** Corresponding author.
E-mail addresses: bntripathi@yahoo.co.in (B.N. Tripathi), sbarua06@gmail.com (S. Barua), naveenkumar.icar@gmail.com (N. Kumar).
[1] Current address. Indian Council of Agricultural Research, Krishi Bhawan, New Delhi, India.

https://doi.org/10.1016/j.antiviral.2021.105232
Received 8 September 2021; Received in revised form 22 November 2021; Accepted 23 December 2021
Available online 29 December 2021

1-associated protein). The writers bind to short consensus sequence motifs in the target mRNA. m6A can be reversibly removed by demethylases (erasers) such as FTO (fat mass and obesity-associated protein) and ALKBH5 (alkylation repair homolog protein 5). m6A is widely distributed along the mRNA, although it is enriched around the stop codons and at the 3′ untranslated regions (UTRs) (Dominissini et al., 2012; Meyer et al., 2012). Readers, such as YTH-domain family 2 (YTHDF2) and heterogeneous nuclear ribonucleoproteins (hnRNPs), directly or indirectly recognise the m6A-marked transcripts and affect various aspects of mRNA metabolism, including RNA localization, splicing, stability (degradation) and translation. Modifications of cap-adjacent nucleotides are deposited to the 5′-ends of RNAs transcribed by RNA polymerase II. Typically, the cap consists of a 7-methylguanosine (m7G) moiety added in a characteristic 5′–5′ triphosphate linkage to the first transcribed nucleotide. The first and second nucleotides adjacent to the cap can be 2′-O-methylated at the ribose sugar (cOMe) in animals, protists and viruses (Galloway and Cowling, 2019). While the m7G is essential for RNA translation and stability (Trotman et al., 2017), the cOMe of mRNA cap is implicated in the innate host antiviral responses (Daffis et al., 2010).

RNA modifications are found in all domains of life viz; animals, plants and their associated pathogens and have been linked to development, health and diseases (Anreiter et al., 2021). m6A modifications have also been observed in diverse groups of viruses including severe acute respiratory syndrome coronavirus 2 (SARS-CoV-2) (Liu et al., 2021). Depending on the nature of the virus involved, m6A modifications may either support (Kennedy et al., 2017; Lichinchi et al., 2016a; Tirumuru et al., 2016) or inhibit (Gokhale et al., 2016; Lichinchi et al., 2016b) viral gene expression. Recent studies have mapped eight m6A sites in SARS-CoV-2 genome (Burgess et al., 2021; Li et al., 2021; Liu et al., 2021) and have suggested that m6A pathway positively regulates virus replication. In this study, we extend the role of methylation by elucidating its novel functions in SARS-CoV-2 life cycle (translation-to-replication switch) and propose that inhibition of methylation by chemical inhibitor (DZNep) may provide therapeutic effect against SARS-CoV-2 without inducing an antiviral drug-resistant phenotype.

2. Material and methods

2.1. Cells

African green monkey kidney (Vero) cells, available at the National Centre for Veterinary Type Cultures (NCVTC), Hisar were grown in Minimum Essential Medium (MEM) supplemented with 10% fetal bovine serum (FBS) (Sigma, St. Louis, USA) and antibiotics (Penicillin and Streptomycin).

2.2. Virus

Wild type (SARS-CoV-2/Human-tc/India/2020/Hisar-4907) and Delta variant (SARS-CoV-2/Human-tc/India/2021/Hisar-177405) of SARS-CoV-2, isolated previously by our group were available at NCVTC, Hisar. Whole genome sequence data of wild type virus is available with GenBank Accession Number of MW555598 while those of Delta virus is having GenBank Accession Number of OL966477.1. Virus was propagated in Vero cells in the Biosafety level 3 (BSL-3) laboratory of ICAR-National Research Centre on Equines (NRCE), Hisar, India. The virus was quantified by plaque assay and viral titres were measured as plaque forming unit per millilitre (PFU/ml) (Kumar et al., 2021).

2.3. Inhibitor

3-Deazaneplanocin A (DZNep) was procured from BioGems International Inc. (Westlake Village, CA, USA) and dissolved in dimethyl sulfoxide (DMSO).

2.4. Antibodies

N6-Methyladenosine (m6A) (D9D9W) Rabbit mAb, METTL3 (E3F2A) Rabbit mAb and hnRNP A1 (D21H11) Rabbit mAbs were received from Cell Signalling Technology (Massachusetts, USA). eIF4E monoclonal antibody (5D11) and Phospho-eIF4E (Ser209) polyclonal antibodies were received from Invitrogen (South San Francisco, CA, USA). Mouse anti-GAPDH (Glyceraldehyde 3-phosphate dehydrogenase, house-keeping control protein) primary antibody, Anti-Mouse IgG (whole molecule)−Alkaline Phosphatase antibody (produced in goat) and Anti-Rabbit IgG (whole molecule)–Peroxidase antibody (produced in goat) was received from Sigma-Aldrich (St. Louis, USA). Rabbit anti-human IgG–HRP was procured from GeNei™, Peenya (Bangalore, India). Human serum from a COVID-19 confirmed patient was received from the civil hospital, Hisar (Haryana).

2.5. Determination of cytotoxicity and virucidal activity of DZNep

The cytotoxic and virucidal effects of DZNep were determined as described previously by our group (Khandelwal et al., 2017).

2.6. Quantitative real-time PCR (qRT-PCR)

Until specified, viral RNA was extracted by QIAamp Viral RNA Mini Kit (Qiagen, Hilden, Germany). cDNA was synthesized as per the protocol described by the manufacturer (Fermentas, Hanover, USA) using either oligo dT (for detection of viral mRNA), random hexamer (for detection of total RNA) or SARS-CoV-2-specific primers as per the requirement. qRT-PCR was carried out to amplify SARS-CoV-2 “N” gene (Forward primer: 5′-ATACAATGTAACACAAGCTTTC-3′ and reverse primer: 5′- AGCAAAATGACTTGATCTTTG-3′) in a 20 μl reaction mixture containing gene-specific primers, template, and iTaq™ Universal SYBR® Green Supermix (Bio-Rad, USA) and has been previously described by our group (Kumar et al., 2021).

2.7. Quantitation of m6A methylome in SARS-CoV-2 infected cells

Quantification of m6A modified RNA was carried out by using EpiQuik™ m6A RNA Methylation Quantification Kit (Colorimetric) (EpiGentek, Farmingdale, NY) as per the protocol described by the manufacturer. Briefly, the RNA was isolated by TRI reagent (Sigma–Aldrich Steinheim, Germany). The isolated RNA along with negative and positive controls (supplied with the kit) were diluted in TE buffer and allowed to bind in the 8-Well Assay Strips in presence of binding solution. The RNA bound to the individual well of Assay Strips was detected using capturing (primary) and detecting (secondary) antibodies. The optical densities (OD) were taken at 450 nm in the microplate reader (Multiskan GO, Thermo Fisher Scientific, Helsinki, Finland). The OD values were normalized with negative controls and the absolute amount of m6A modified RNA (%) was calculated by comparing with the positive control.

2.8. CHIP assay

CHIP assay was carried out to evaluate the interaction of viral RNA/mRNA with cellular proteins viz. cap-binding protein (eIF4E) and hnRNPA1 as per the previously described method (Kumar et al., 2021) with some modifications. Briefly, Vero cells, in triplicates were infected with SARS-CoV-2 at MOI (multiplicity of infection) of 5. At indicated time post-infection, the cells were treated with 1% formaldehyde for 10 min to covalently cross-link interacting proteins and nucleic acid. Thereafter, the cross-linking reaction was stopped by the addition of 125 mM glycine, followed by washing the cells with ice-cold PBS. The cells lysates were prepared in immunoprecipitation (IP) buffer [150 mM NaCl, 50 mM Tris-HCl (pH 7.5), 5 mM EDTA, 0.5% NP-40, 1% Triton X-100 plus protease and phosphatase inhibitor cocktail] and sonicated

in a Qsonica Sonicator Q500 (Qsonica, Newtown, CT, USA) (6 pulse of 15 s at an amplitude of 40%). The sonicated cell lysate was centrifuged for 10 min at 12,000g. The clarified cell lysate was mixed with 10 units of RiboLock RNase Inhibitor (Thermo Scientific, USA) and then incubated with primary antibody or an equivalent volume of IP buffer (beads control) for 45 min at room temperature. Thereafter, 40 μl (5 ng/μl) of Protein A Sepharose® slurry, prepared as per the instruction of the manufacturer (Abcam, USA) was added into each reaction and incubated overnight at 4°C on a rotary platform. The beads were then washed 5 times in the IP buffer. In order to reverse the cross-linking, the complexes were incubated with proteinase K (20 mg/ml final concentration) at 56°C for 40 min. Finally, the reaction mixture was centrifuged at 2000 g for 1 min and the purified RNA (TRI reagent) from the supernatant was subjected to cDNA preparation and quantitation of SARS-CoV-2 RNA (N gene) by qRT-PCR.

2.9. 5' cap synthesis assay

To evaluate the effect of DZNep on the synthesis of the 5' cap of viral mRNA, a cell free interaction assay between viral mRNA and purified eIF4E protein was performed as described previously (Choi and Hagedorn, 2003; Masse et al., 2014; Schwartz and Parker, 2000). Briefly, uninfected Vero cell lysate, prepared with a non-denaturing agent was incubated with Protein A Sepharose beads to allow its binding with α-peIF4E. The unbound α-peIF4E was removed by washing with IP buffer and stored at −70°C in a deep freezer. Next, Vero cells, in triplicates were infected with SARS-CoV-2 at MOI of 5. DZNep or vehicle control was added at 3 hpi. Subsequently, cells were lysed at 8 hpi and subjected to RNA extraction using TRI reagent. An equal amount of viral RNA (normalized by qRT-PCR) was then incubated with the complex containing peIF4E-αpeIF4E-Protein A Sepharose complex for 30 min in IP buffer. The complex was then subjected to centrifugation at 2000*g* for 2 min and washed 5 times with PBS. The pellet was subjected to RNA extraction using TRI reagent, followed by cDNA preparation (using oligo dT) and quantitation of SARS-CoV-2 mRNA (N gene) by qRT-PCR.

2.10. Cross linking immunoprecipitation (CLIP) assay

Cross-linking immunoprecipitation was conducted as described previously with some modifications (McHugh et al., 2015; Ramanathan et al., 2019). Confluent monolayers of Vero cells were infected with SARS-CoV-2 at MOI of 5 for 1h in the presence of DZNep or vehicle control, followed by washing with PBS and the addition of fresh MEM having either DZNep or vehicle control. At 2 hpi, cells were treated for 10 min with 1% formaldehyde to covalently cross-link the interacting proteins and nucleic acid. Thereafter, the cross-linking reaction was stopped by addition of 125 mM glycine (final concentration), followed by washing the cells with ice-cold PBS. The cells lysates were prepared by incubating cells with 1 ml of IP buffer [150 mM NaCl, 50 mM Tris-HCl (pH 7.5), 5 mM EDTA, 1% NP-40 plus protease and phosphatase inhibitor cocktail] for 10 min. Thereafter, the cell lysate was subjected to low centrifugation (1000*g* for 10 min). The top 1/3rd portion (~300 μl), called the cytosolic fraction, was collected in a fresh tube and clarified again by centrifugation at 6000*g* for 10 min (Suzuki et al., 2010). The pellet was discarded and the clarified cytosolic fraction was mixed with 10 units of RiboLock RNase inhibitor, protease and phosphatase inhibitor cocktail and incubated with the Protein A Sepharose-bound m6A specific primary antibody (reactive antibody), Protein A Sepharose bound-phospho ERK antibody (non-reactive antibody) or an equivalent volume of IP buffer (beads control) overnight at 4 °C on a rotary platform. Finally, the reaction mixture was centrifuged at 2000g for 1 min and washed five times with PBS. The precipitated protein-RNA complex was resuspended in 100 μl PBS for quantification of the m6A-bound proteins (Western blot analysis).

2.11. siRNA knockdown

Vero cells, in triplicates, were grown at ~75% confluency in 6 well plates and transfected with target- or negative control siRNAs (Table S1) using Lipofectamine 3000 as per the manufacturer's (Invitrogen, Carlsbad, USA) instruction. At 48 h post-transfection, cells were infected with SARS-CoV-2 at MOI of 1 and the viruses released in the infected cell culture supernatant at 24 hpi was quantified by plaque assay. The cell pellet was subjected to Western blot analysis to probe the respective cellular proteins.

2.12. Determination of the lethal dose 50 (LD_{50}) of DZNep in embryonated chicken eggs

To determine LD_{50}, 100 μl of 5-fold serial dilutions (500-5 μg/egg) of DZNep (3 eggs/dilution) or equivalent volumes of DMSO (vehicle control) were administered in specific pathogen free (SPF) embryonated chicken eggs via allantoic route. The eggs were observed daily for mortality of the embryos. The LD_{50} was determined by Reed-Muench method.

2.13. In ovo antiviral efficacy of DZNep against IBV

SPF embryonated chicken eggs, in triplicates, were inoculated with either 5 μg or 25 μg of DZNep or equivalent volume of DMSO via allantoic route and subsequently infected with IBV at egg infective dose 50 (EID_{50}) of 100. The eggs were visualized daily for up to 6 days post-inoculation for mortality of the embryos. Effective concentration 50 (EC_{50}) was determined by the Reed-Muench method.

2.14. Statistical analysis

Pairwise statistical comparisons were performed by two-tailed Student's t-test in GraphPad Prism 8.0 software.

3. Results

3.1. m6A modifications facilitate SARS-CoV-2 replication

We screened a library of small molecule chemical inhibitors and identified DZNep as an inhibitor with anti-SARS-CoV-2 activity. DZNep is known to act as inhibitors of S-adenosylhomocysteine (SAH) hydrolase and, as a result, to deplete cells of S-adenosylmethionine (SAM), the methyl donor used by METTL3 and several other writers. At the non-cytotoxic concentrations (Fig. 1a), DZNep exhibited anti-SARS-CoV-2 activity in a dose-dependent manner (Fig. 1b). Since DZNep did not exert any virucidal effect, anti-SARS-CoV-2 activity of DZNep could be a result of the inhibition of SARS-CoV-2 replication in the target cells, rather than the inactivation of cell free virions (Fig. S1). Furthermore, siRNA knockdown of m6A writers (METTL3) (Fig. S2a), m6A reader (hnRNPA1) (Fig. S2b) and MAT2A-the enzyme involved in synthesizing universal methyl donor (SAM) (Fig. S2c) resulted in a decreased virus yield (Fig. 1c, d and 1e), suggesting that m6A epitranscriptomic machinery positively regulates SARS-CoV-2 replication. Moreover, DZNep was also shown to block replication of the Delta variant of SARS-CoV-2 (Fig. 1f), suggesting, as an antiviral agent, it may act against multiple SARS-CoV-2 variants. In addition, DZNep was also shown to exhibit its antiviral effects in BHK-21 cells (other than Vero cells) (Fig. 1g).

3.2. Reprogramming of m6A methylome in SARS-CoV-2 infected cells

Like other RNA viruses, coronavirus RNA also undergoes epitranscriptomic changes in virus infected cells. A recent study on transcriptome-wide characterization of m6A methylome of SARS-CoV-2 infected cells suggests that m6A sites are widely distributed across the viral RNA (Liu et al., 2021), although the precise role of these

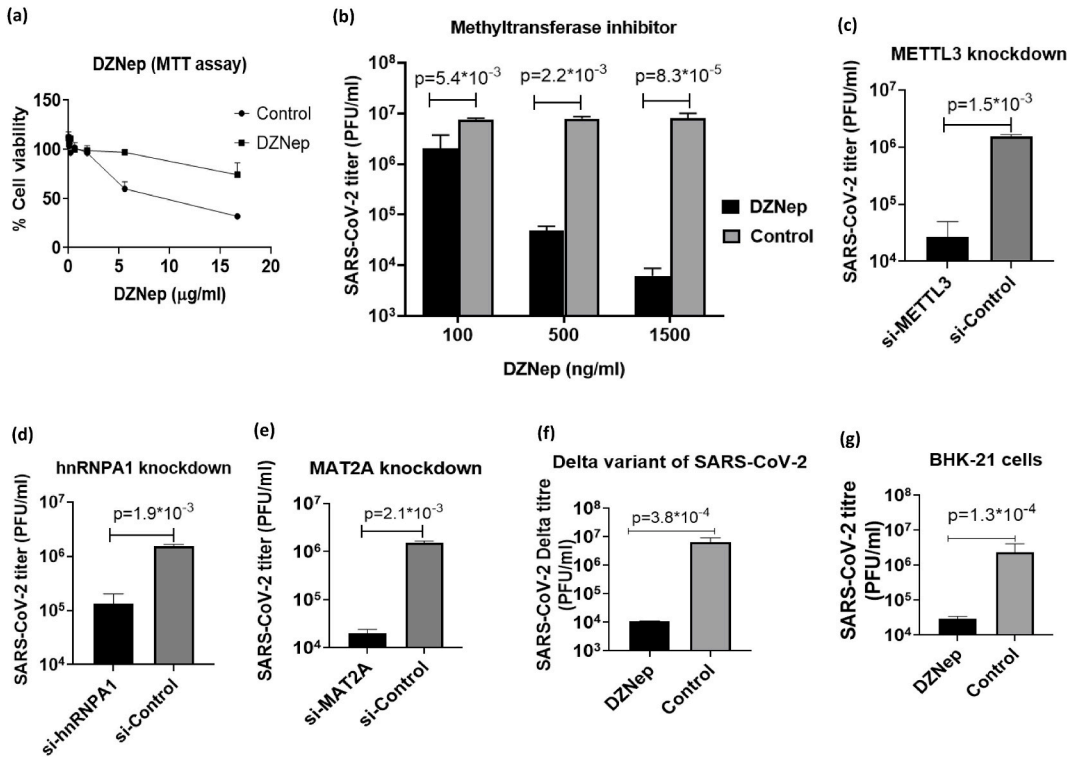

Fig. 1. m6A modifications positively regulate SARS-CoV-2 replication. ***(a) Determination of the* Cytotoxicity of DZNep.** Indicated concentrations of DZNep or equivalent volumes of vehicle control (DMSO) were incubated with cultured Vero cells for 96 h and % cell viability was measured by MTT assay. **(b).** ***DZNep inhibits SARS-CoV-2 replication.*** Vero cells, in triplicates, were infected with SARS-CoV-2 at MOI of 0.1 in the presence of indicated concentrations of DZNep or vehicle-control. The virus particles released in the infected cell culture supernatants at 48 hpi were quantified by plaque assay. ***(c-e) siRNA knockdown.*** Vero cells, in triplicates, were transfected with indicated siRNAs along with negative control, followed by SARS-CoV-2 infection at MOI of 1. The virus yields in the infected cell culture supernatants at 24 hpi were quantified by plaque assay. The virus yield in *METTL3* ***(c),*** *hnRNPA1* ***(d)*** and *MAT2A* ***(e)*** knockdown cells is shown. ***(f) Antiviral efficacy of DZNep against Delta variant of SARS-CoV-2.*** 1 μg/ml of DZNep was used to assess its antiviral efficacy against Delta variant of SARS-CoV-2. ***(g) Antiviral efficacy of DZNep in BHK 21 cells.*** Antiviral efficacy of DZNep at a non-cytotoxic concentration (1 μg/ml) against SARS-CoV-2 (MOI = 0.1) carried out in BHK-21 cells is shown. Values are means ± SD and representative of the result of at least 3 independent experiments. p value indicates the level of statistically significant difference.

epitranscriptomic marks on the viral genome is yet to be elucidated. We evaluated the kinetics of m6A modifications during the course of SARS-CoV-2 infection in Vero cells wherein cell lysates from SARS-CoV-2-infected cells were subjected to immunoprecipitation using α-m6A, followed by quantitation of viral RNA by qRT-PCR.

The levels of viral RNA immunoprecipitated by α-m6A varied (Fig. 2a). The peak levels could be detected at 10 hpi-12 hpi (Fig. 2a). Interestingly, at 2 hpi, the relative levels of m6A-modified SARS-CoV-2 RNA was significantly higher (~10%) than at 1 hpi (~5%), 4 hpi (~5%) and 6 hpi (~4%) (Fig. 2a). This indicates that SARS-CoV-2 RNA is subjected to m6A modifications in the infected cells and this modification is a dynamic event (Fig. 2a).

In addition to determining the relative levels of m6A-marked RNA during the course of SARS-CoV-2 replication cycle, we also examined the absolute levels (ratio of m6A-modified RNA versus total RNA) of m6A-marked RNA by EpiQuik m6A RNA Methylation Quantification Kit. In non-infected (mock-infected) cells ~0.03% of the total cellular RNA was found to be methylated whereas in SARS-CoV-2-infected cells, it varied from 0.02 to 0.09%, depending on the stage of the virus replication cycle involved-the highest being at middle-late step of virus replication cycle (3 hpi to 10 hpi) and lowest during the initial hours of infection (1 hpi and 2 hpi) (Fig. 2b). No detectable amount of methylation was observed in RNA derived from cell-free virions (Fig. 2b). Addition of DZNep significantly reduced the levels of methylated RNA (Fig. 2c). Taken together, it could be concluded that SARS-CoV-2 RNA is subjected to m6A modifications in the target cells and these modifications are removed before the formation of mature virion particles.

3.3. DZNep reduces levels of SARS-CoV-2 RNA

SARS-CoV-2 life cycle is ~10 h in cultured Vero cells (Kumar et al., 2021). In order to evaluate which specific step(s) of SARS-CoV-2 life cycle are affected, DZNep was applied at various times post-infection and the progeny virus particles released at 12 h were quantified. Addition of DZNep had similar levels of suppression in virus yield whether it was applied at 30 min before- or 1 h after virus infection (Fig. 3a), suggesting that DZNep had no effect on the early steps of SARS-CoV-2 replication. Likewise, there was no inhibitory effect if it was applied at later time points (≥6 hpi) of SARS-CoV-2 life cycle which suggested that DZNep does not target the SARS-CoV-2 budding/release. The magnitude of the inhibitory effect of DZNep on SARS-CoV-2 replication decreased from 1 hpi to 6 hpi, suggesting that DZNep most likely targeted the middle stages (replication/transcription/translation) of SARS-CoV-2 replication. In order to further confirm the specific steps of SARS-CoV-2 targeted by the inhibitors, we conducted the virus step-specific assays (Kumar et al., 2021). The DZNep did not affect the SARS-CoV-2 attachment, entry and budding (data not shown). To evaluate the effect of the DZNep on the synthesis of viral genome, it was applied at 3 hpi (a time point when early steps of viral life cycle such as attachment and entry are expected to occur) and the cell lysates were prepared at 10 hpi, a time point when virus is close to completing its life cycle. DZNep-treated cells exhibited significantly low levels of mRNA (Fig. 3b1) and total RNA (Fig. 3b2), suggesting that the m6A modifications could be essential for the optimal synthesis of SARS-CoV-2 genome.

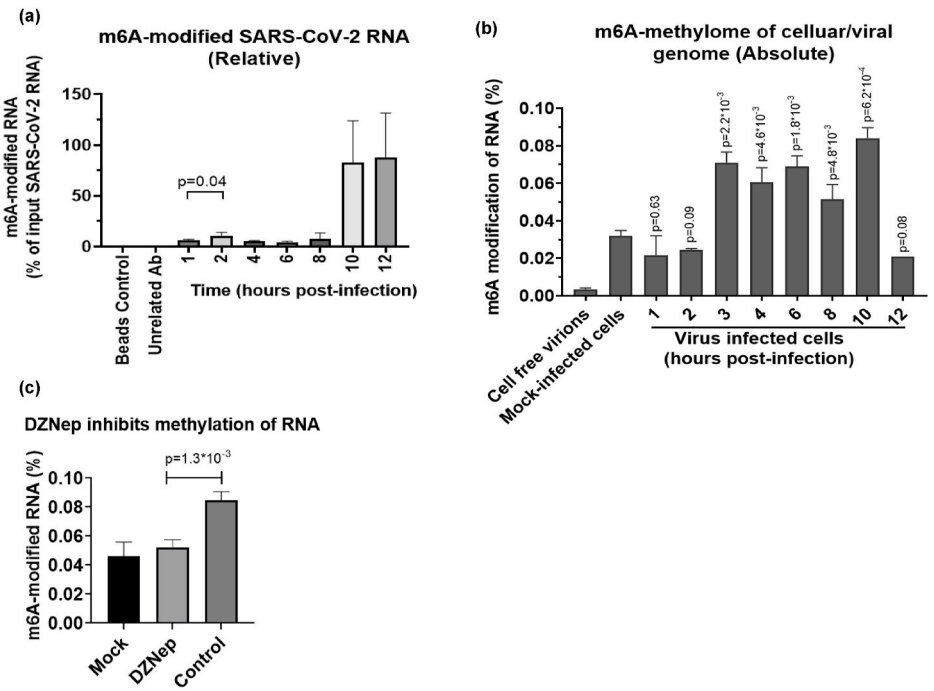

Fig. 2. SARS-CoV-2 infection leads to reprogramming of m6A methylome ***(a) Kinetics of the m6A modification in SARS-CoV-2 genome.*** Vero cells, in triplicates were infected with SARS-CoV-2 at MOI of 5 followed by washing with PBS and addition of fresh MEM. Cell lysates were prepared at the indicated time points and subjected to CHIP assay. The cell lysates were incubated with α-m6A to immunoprecipitate the m6A-modified RNA. The levels of SARS-CoV-2 RNA ("N" gene) at different time points were quantified by qRT-PCR and expressed as % of the input viral RNA. ***(b) Quantitation of m6A methylome.*** Five hundred millilitre of virus (SARS-CoV-2 infected cell culture supernatant) was filtered using 0.45 μm syringe filter, treated with RNase A and DNAse-I to eliminate the uncapsidated cellular RNA/DNA and then ultracentrifuged at 30,000 rpm for 1 h. The resulting pellet was resuspended in 1 ml PBS. Purified virus particles and **c**ell lysates from mock- or SARS-CoV-2-infected cells at indicated time points were subjected to RNA isolation. Equal amount of RNA was evaluated for the determination of the absolute level of m6A modified RNA by EpiQuikTM m6A RNA Methylation Quantification Kit (Colorimetric). The OD values were normalized with negative controls and absolute amount of m6A modified RNA (%) was calculated by comparing it with the positive control. ***(c) DZNep inhibits methylation of RNA.*** Vero cells, in triplicates were infected with SARS-CoV-2 at MOI of 5 followed by washing with PBS and addition of DZNep (1 μg/ml) or 0.05% DMSO. Cell lysates were prepared at 10 hpi. Equal amount of total RNA was evaluated for the determination of the absolute level of m6A modified RNA by EpiQuik™ m6A RNA Methylation Quantification Kit as described above. Values are means ± SD and representative of the result of at least 3 independent experiments. p value indicates the level of statistically significant difference.

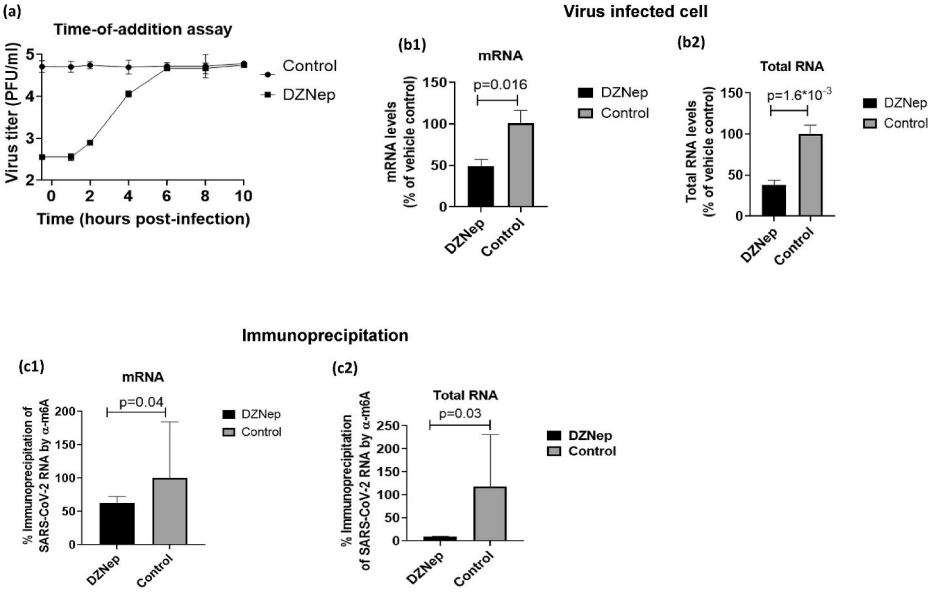

Fig. 3. m6A modifications facilitate synthesis of SARS-CoV-2 genome.

(a) Time-of-addition-addition assay. Confluent monolayers of Vero cells, in triplicate, were infected, with SARS-CoV-2 at MOI of 5 for 1 h, washed 6 times with PBS and fresh medium with either DZNep (1 μg/ml) or 0.05% DMSO was added at indicated times. Supernatant was collected at 12 hpi and quantified by plaque assay. ***(b) Effect of DZNep on synthesis of viral RNA.*** Confluent monolayers of Vero cells, in triplicates, were infected with SARS-CoV-2 for 1 h at MOI of 5. DZNep (1 μg/ml) was added at 3 hpi and cells were harvested at 10 hpi to determine levels of SARS-CoV-2 RNA by qRT-PCR. Oligo dT and random hexamer primers were used to detect mRNA and total RNA respectively. Threshold cycle (Ct) values were analyzed to determine relative fold-change in copy numbers of mRNA **(b1)** and total RNA (**b2**). ***(c) m6A modifications are essential for synthesis of SARS-CoV-2 genome.*** Vero cells, in triplicates were infected with SARS-CoV-2 at MOI of 5 followed by washing with PBS and addition of fresh MEM. DZNep (1 μg/ml) or equivalent volume of vehicle control were applied at 3 hpi and cell lysates were prepared at 8 hpi to isolate the RNA. Equal amount of SARS-CoV-2 RNA (normalized by qRT-PCR) was incubated with α-m6A to immunoprecipitate the m6A-modified RNA. The amount of SARS-CoV-2 RNA in the immunoprecipitate was quantified by qRT-PCR. Threshold cycle (Ct) values were analyzed to determine relative fold-change (% of vehicle control) in copy numbers of mRNA ***(c1)*** and total RNA **(*c2*)**. Values are means ± SD and representative of the result of at least 3 independent experiments. p value indicates the level of statistically significant difference.

In order to confirm the association of m6A marks in synthesizing viral RNA, the cell lysates were immunoprecipitated by α-m6A and quantified by qRT-PCR. The amount of SARS-CoV-2 RNA immunoprecipitated by α-m6A was significantly low in the cells treated with DZNep [Fig. 3c1 (mRNA) and 3c2 (Total RNA)] suggesting that m6A-modifications of SARS-CoV-2 RNA are essential for optimal

synthesis of the SARS-CoV-2 genome.

3.4. DZNep inhibits interaction of hnRNPA1and m6A-modified SARS-CoV-2 RNA

A previous study on the SARS-CoV-2 has mapped eight m6A sites in the viral genome (Liu et al., 2021). In order to predict the putative m6A writers (RNA binding proteins), we analyzed the SARS-CoV-2 genome (SARS-CoV-2/Human-tc/India/2020/Hisar-4907, bearing Accession Number VTCCAVA294 and GenBank Accession number MW555598) in the RNA-binding protein database (RBPDB) (http://rbpdb.ccbr.utoronto.ca). Out of the 11 m6A readers known (Zhao et al., 2020), *in silico* binding with the SARS-CoV-2 genome could be predicted with only hnRNPA1 and YTHDC1. The hnRNPA1 was predicted to bind in the 3′-end (two sites) and "S" gene (one site) of the SARS-CoV-2 genome with a position weight matrix score of >9.89 (Table S2). The YTHDC1 was predicted to interact at multiple sites in each gene (except ORF6, ORF7a and ORF7 where no binding sites could be predicted) of SARS-CoV-2, although the position weight matrix score for all the sites was low (<6.5).

Next we evaluated the functional role of hnRNPA1 in SARS-CoV-2 life cycle. SARS-CoV-2 infection in Vero cells resulted in a biphasic expression of hnRNPA1 (Fig. 4a). The first and second peaks could be observed at 2–4 hpi and 6–8 hpi respectively (Fig. 4a). The CHIP assay using α-hnRNPA1 immunoprecipitated the SARS-CoV-2 RNA, suggesting it's direct interaction with the SARS-CoV-2 RNA (Fig. 4b). The DZNep-treatment resulted in a decrease in the SARS-CoV-2 RNA, immunoprecipitated by α-hnRNPA1 (Fig. 4b) which suggested that m6A modifications facilitates interaction of hnRNPA1 with viral RNA to optimally synthesize viral genome. Further, DZNep did not directly affect the levels of hnRNPA1 expression (Fig. 4c) suggesting that the inhibitory effect of DZNep is mediated via the RNA-protein interaction rather than by the reduced hnRNPA1 expression.

3.5. Methylation of the 5' cap of SARS-CoV-2 mRNA is essential for eIF4E-mediated translation of viral proteins

Besides inhibiting RNA synthesis, DZNep treatment also resulted in reduced levels of SARS-CoV-2 proteins in the infected cells (Fig. 5a). In coronaviruses, viral mRNA translation takes place in a cap-dependent manner wherein the eIF4E plays a central role in the initiation of translation (Kumar et al., 2021). Upon phosphorylation by the upstream kinase(s), elF4E binds to the 5′ cap of mRNA to initiate translation (Kumar et al., 2021). Besides internal RNA modifications, the 5′-cap of coronaviruses also undergoes epitranscriptomic changes which include m7G and cOMe (Imam et al., 2020; Liu et al., 2021). The SAM serves as a methyl donor in both these reactions. We further explored if DZNep-induced perturbation of epitranscriptomic changes may affect interaction of the viral mRNA and eIF4E. At 8 hpi (when SARS-CoV-2 RNA was expected to be at its peak level), cells were covalently cross-linked and evaluated for viral RNA and eIF4E interaction in a CHIP assay. In agreement with our previous findings (Kumar et al., 2021), α-eIF4E (reactive antibody) but not α-ERK (non-reactive antibody) or beads control immunoprecipitated SARS-CoV-2 RNA (Fig. 5b). The levels of viral RNA immunoprecipitated by α-eIF4E were ~99.9% lower in DZNep-treated cells as compared to the vehicle-control-treated cells (Fig. 5b) which suggested that DZNep inhibits eIF4E/SARS-CoV-2 mRNA interaction which may eventually result in the decreased synthesis of viral protein. In qRT-PCR, the levels of SARS-CoV-2 RNA in α-ERK-treated cells (but not α-eIF4E-treated cells) were undetectable which clearly indicated that α-eIF4E specifically interacted with SARS-CoV-2 RNA (Fig. 5b).

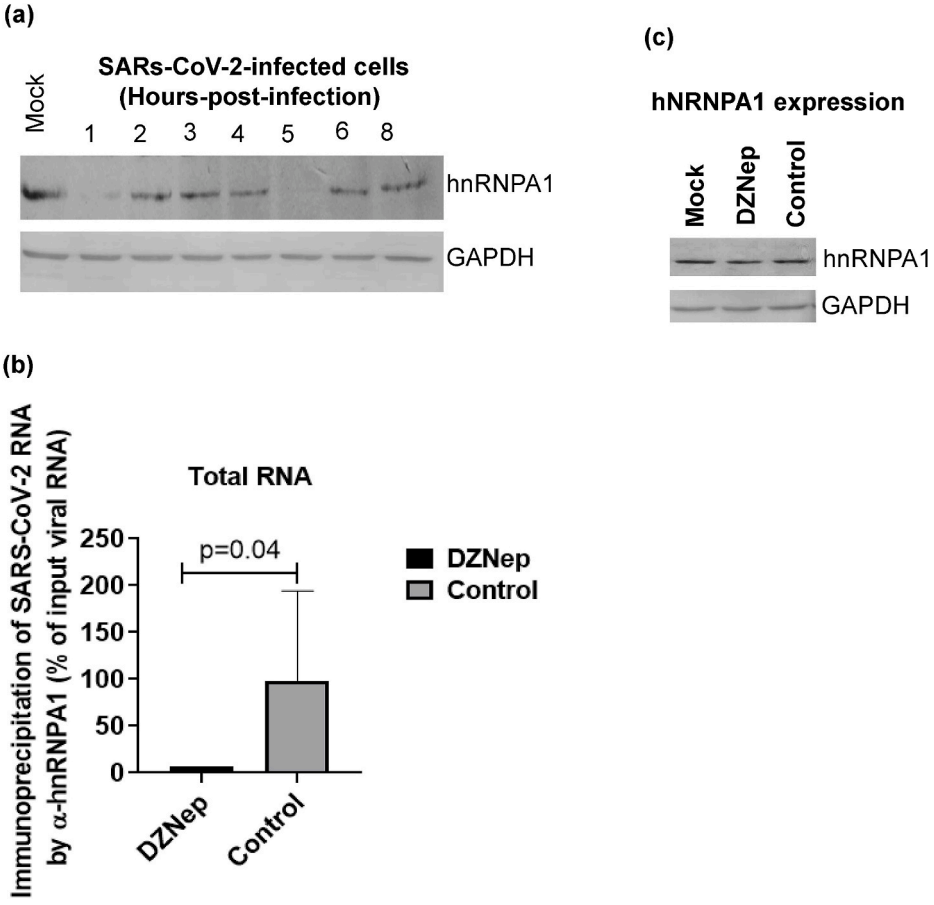

Fig. 4. m6A modifications facilitate binding of hNRNPA1 with viral RNA to optimally synthesize viral genome. ***(a) Kinetics of hnRNPA1 expression in SARS-CoV-2-infected Vero cells.*** Vero cells were infected with SARS-CoV-2 at MOI of 5 and the cell lysates were prepared at the indicated time points to determine the levels of hnRNPA1 and GAPDH in a Western blot analysis. ***(b) hnRNPA1 interacts with m6A-modified SARs-CoV-2 RNA and this interaction is essential for optimal synthesis of the viral genome.*** Vero cells, in triplicates were infected with SARS-CoV-2 at MOI of 5 followed by washing with PBS and addition of fresh medium. DZNep (1 μg/ml) or equivalent volume of vehicle control were applied at 3 hpi and cell lysates were prepared at 10 hpi, Cell lysates were incubated with α-hnRNPA1 to immunoprecipitate the RNA associated with it. The relative levels of SARS-CoV-2 RNA (N gene) in the immunoprecipitate were determined by qRT-PCR and expressed as % of the input viral RNA. ***(c) Effect of DZNep on hnRNPA1 expression.*** Vero cells were infected with SARS-CoV-2 at MOI of 5 and the cell lysates were prepared at 3 hpi to determine the levels of hnRNPA1 and GAPDH in a Western blot analysis. Values are means ± SD and are representative of the result of at least 3 independent experiments. p value indicates the level of statistically significant difference.

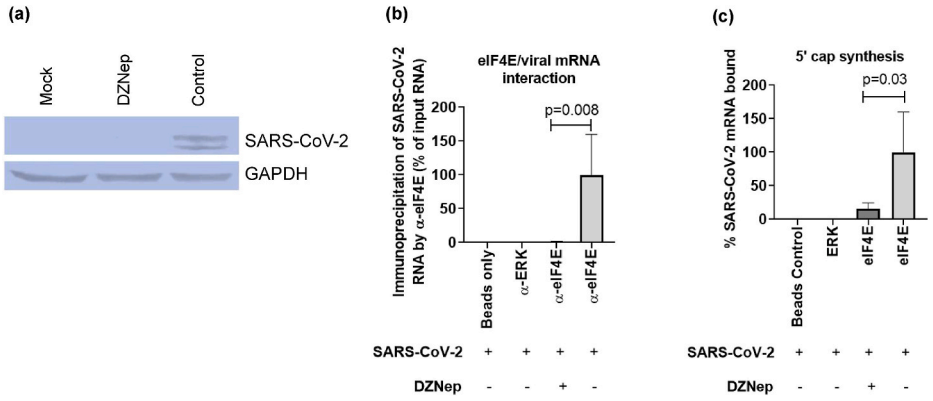

Fig. 5. Methylation of the cap-adjacent nucleotides in the 5′ cap of SARS-CoV-2 mRNA is essential for eIF4E-mediated translation of viral proteins. ***(a) Effect of DZNep on synthesis of SARS-CoV-2 protein.*** Vero cells were infected with SARS-CoV-2 at MOI of 5. DZNep (1 μg/ml) or equivalent volume of vehicle control were added at 3 hpi. Cell lysates were prepared at 8 hpi to detect the levels of viral proteins by Western blot analysis by using serum from a COVID-19-infected patient. The levels of viral proteins **(upper panel)**, along with housekeeping GAPDH protein (**lower panels**) are shown. ***(b) Cap-adjacent epitranscriptomic modifications in the 5′ cap of SARS-CoV-2* mRNA *djacent epitranscriptomic modifications in the 5′ cap of SARS-CoV-2* mRNA *are essential for interaction with eIF4E.*** Vero cells, in triplicates were infected with SARS-CoV-2 at MOI of 5 followed by washing with PBS and addition of fresh MEM. DZNep (1 μg/ml) or equivalent volume of vehicle control were applied at 4 hpi and cell lysates were prepared at 8 hpi, Cell lysates were incubated with α-eIF4E to immunoprecipitate the RNA. The amount of SARS-CoV-2 RNA in the immunoprecipitate was quantified by qRT-PCR and expressed as % of input viral RNA. ***(c) DZNep leads to defective synthesis of the 5′ cap of viral mRNA.*** The p-eIF4E was purified from uninfected Vero cells as described in the material and method section. Next, Vero cells, in triplicates were infected with SARS-CoV-2 at MOI of 5 followed by washing with PBS and addition of fresh MEM. DZNep (1 μg/ml) or equivalent volume of vehicle control(s) were applied at 3 hpi. At 8 hpi, cells were subjected to RNA extraction using TRI reagent. Equal amount of viral RNA from DZNep and vehicle control-treated cells (RNA levels were normalized by qRT-PCR) were incubated with purified p-eIF4E (described above) for 30 min. The immunoprecipitate was subjected to RNA extraction, cDNA preparation (using oligo dT) and quantitation of SARS-CoV-2 mRNA (N gene) by qRT-PCR. Values are means ± the result of at least 3 independent experiments. **=$p < 0.01$, *=$p < 0.05$. p value indicates the level of statistically significant difference

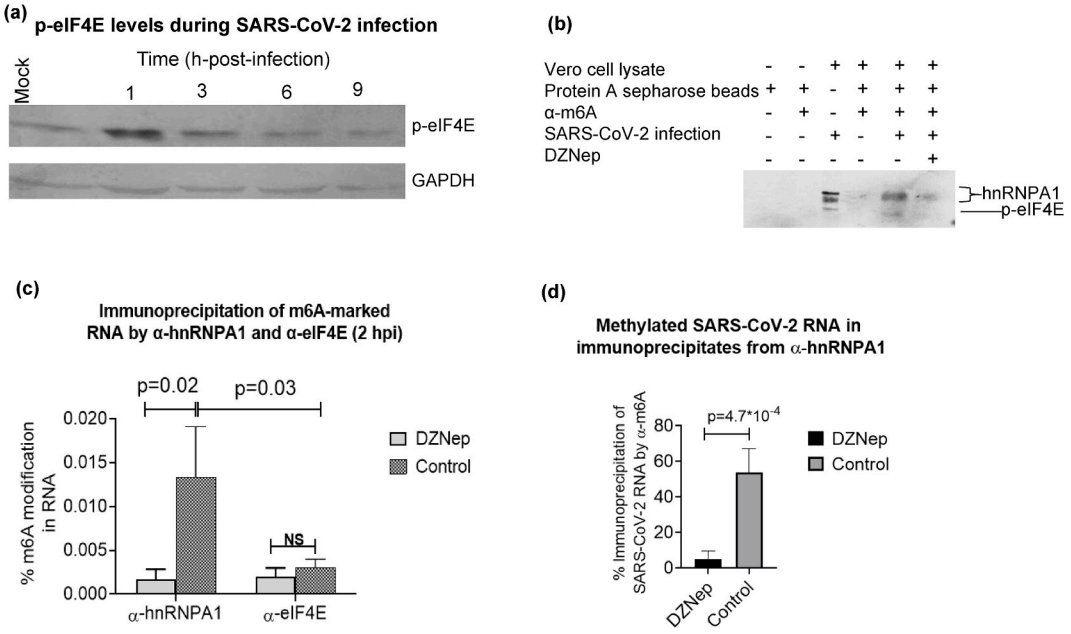

Fig. 6. m6A modifications of viral RNA act as a molecular switch from translation to replication of SARS-CoV-2 RNA. ***(a) Kinetics of eIF4E activation in SARS-CoV-2-infected cells.*** Vero cells were infected with SARS-CoV-2 at MOI of 5 and the cell lysates were subjected to determination of the levels of p-eIF4E and GAPDH in a Western blot analysis at indicated time points. ***(b) Levels of α-hnRNPA1 and α-eIF4E in the cell lysate immunoprecipitated by α-m6A***. Confluent monolayers of Vero cells were infected with SARS-CoV-2 at MOI of 5 for 1 h, followed by washing with PBS and the addition of fresh MEM having DZNep (1 μg/ml) or equivalent volume of DMSO. At 2 hpi cells were subjected to covalently cross-link proteins and nucleic acid for 10 min. The cells lysates and cytosolic fractions were prepared as described in materials and methods under CLIP assay. The cytosolic fraction was subjected to immunoprecipitation by α-m6A. Proteins (hnRNPA1 and eIF4E) interacting with m6A-marked-RNA were probed from the immunoprecipiate (protein-RNA complex) by Western blot analysis. ***(c) Levels of m6A-modifed RNA in the cell lysates (at 2 hpi) immunoprecipitated with α-hnRNPA1 and α-eIF4E.*** Confluent monolayers of Vero cells were infected with SARS-CoV-2 at MOI of 5 for 1h in the presence of DZNep (1 μg/ml) or equivalent volume of DMSO, followed by washing with PBS and the addition of fresh MEM having either DZNep or vehicle control. At 2 hpi, cells were subjected to covalent cross-linking. The cells lysates were then incubated with α-hnRNPA1 or α-eIF4E and the immunoprecipitates were subjected to determination of m6A methylome by EpiQuikTM m6A RNA Methylation Quantification Kit (Colorimetric). (d) ***Levels of m6A-modifed SARS-CoV-2* RNA**. DZNep-treated or vehicle control-treated cells (at 2 hpi) were first immunprecipitated by α-hnRNPA1. The hnRNPA1-bound RNA (immunoprecipitate) was purified (Triazol) and again subjected to immunoprecipitation using α-m6A. The relative levels of m6A-modified SARS-CoV-2 RNA in the immunoprecipitate were quantified by qRT-PCR and expressed as % of input (RNA immunoprecipitated by α-hnRNPA1) SARS-CoV-2 RNA. Values are means ± SD and representative of the result of at least 3 independent experiments. p value indicates the level of statistically significant difference. NS indicates nonsignificant diffference.

Besides inhibiting the interaction between SARS-CoV-2 mRNA and eIF4E, alternatively, the DZNep-mediated decreased synthesis of viral proteins could also be due to defective synthesis of the 5' cap of viral mRNA. We performed a cell-free viral mRNA and cellular phospho-eIF4E (p-eIF4E) interaction assay wherein p-eIF4E (purified from the mock-infected cells lysate using α-peIF4E) was subjected to *in vitro* interaction with SARS-CoV-2 RNA. Since the low levels of viral RNA in DZNep-treated cells could eventually reflect lower levels of immunoprecipitated viral RNA, equal amount of viral RNA from vehicle control- and DZNep-treated cells (normalized by qRT-PCR) was taken for the assay. As compared to the vehicle control-treated cells, the amount of RNA immunoprecipitated by α-peIF4E-peIF4E complex was ~80% lower in cell lysates from DZNep-treated cells (Fig. 5c). This confirmed that perturbation of epitranscriptomic machinery (methylation) produces defective SARS-CoV-2 mRNA which is unable to interact with eIF4E, eventually resulting in decreased synthesis of viral proteins (Kumar et al., 2021).

3.6. m6A modifications regulate the switching from translation to replication of SARS-CoV-2 RNA

SARS-CoV-2 has a positive-sense RNA genome. Immediately upon infection, 2/3rd of the nascent viral RNA is directly translated into 16 non-structural proteins (NSPs) in the cytoplasm of the infected cells (Beig Parikhani et al., 2021). The same nascent viral RNA then switches to act as template for viral RNA transcription. We observed a switch on/off phenomenon in the hnRNPA1 expression levels in SARS-CoV-2 infected Vero cells (Fig. 4a). This tempted us to speculate that hnRNPA1 could be involved in switching from translation to replication of SARS-CoV-2 RNA. At 1 hpi, we could detect low levels of hnRNPA1 (m6A reader) (Fig. 4a) and viral/cellular m6A methylome (Fig. 2a and b) but higher levels of p-eIF4E-the cellular protein that participates in translation) (Fig. 6a). Conversely, at 2 hpi, the levels of methylome (Fig. 2a and b) and hnRNPA1 (Fig. 3a) were significantly higher but the level of p-eIF4E decreased (Fig. 6a). Differential recruitment of translational (p-eIF4E) and transcriptional cellular machinery (m6A/hnRNPA1) respectively at 1 hpi and 2 hpi indicated that these cellular factors may mediate the switching between translation and transcription. Since the recruitment of these epitranscriptomically-regulated cellular factors were dampened in the presence of DZNep, the switching phenomenon could be associated with epitranscriptomic changes of viral mRNA. To provide further insights into this switching phenomenon, SARS-CoV-2-infected Vero cells were cross-linked at 2 hpi and evaluated for the interaction of m6A-modified RNA with RNA-binding proteins (p-eIF4E/hnRNPA1) in a CLIP assay. The hnRNPA1 principally binds at the 3′-end of the SARS-CoV-2 genome (Table S2) whereas the eIF4E is a 5′ mRNA cap-binding protein. Therefore, the sonication step was omitted in the CLIP assay which ensured the recovery of all the RBPs associated with SARS-CoV-2 genome. The cross-linked m6A-modified RNA was immunoprecipitated by α-m6A and the associated RBPs viz; hnRNPA1 and p-eIF4E, were probed in Western blot analysis. At 2 hpi, only hnRNPA1 but not eIF4E was shown to be associated with m6A-modified SARS-CoV-2 RNA, suggesting repression of translation (2 hpi) due to recruitment of hnRNPA1 (Fig. 6b). The amount of hnRNPA1 immunoprecipitated by α-m6A was lower in DZNep-treated cells as compared to the control (Fig. 6b) which suggested a decreased synthesis of SARS-CoV-2 genome due to perturbation of the epitranscriptomic machinery.

To further confirm the association of m6A modifications in regulating the switching from translation to replication, we performed another assay wherein SARS-CoV-2 infected cell lysates were subjected to immunoprecipitation by α-hnRNPA1 and- α-peIF4E, followed by quantitation of m6A RNA methylome in the immunoprecipitates. As shown in Fig. 6c, the amount of m6A-modified total RNA immunoprecipitated by α-hnRNPA1-was much higher than those immunoprecipitated by α-peIF4E, suggesting that hnRNPA1 (but not eIF4E) interacts with m6A-marked RNA or in other words m6A marks on SARS-CoV-2 allows recruitment of RBPs such as hnRNPA1 which represses translation and facilitate transcription. Further, the amount of m6A-modified RNA immunoprecipitated by α-hnRNPA1 was found to be significantly lower in DZNep-treated cells as compared to the vehicle-control-treated cells, suggesting an arrest in RNA synthesis due to perturbation of epitranscriptomic (m6A modification) machinery. These multiple lines of evidence clearly suggest that m6A modifications of viral RNA serve as a molecular switch from translation to replication during early hours of SARS-CoV-2 replication cycle.

3.7. Selection of drug-resistant virus variants

To evaluate the generation of potential DZNep-resistant viral variants, SARS-CoV-2 was passaged 40 times in the presence of DZNep (a host-targeting agent) or vehicle control. When the relative fitness was compared at P40 in the presence of DZNep, P40-DZNep and P40-Control viruses were found to replicate at similar titers in Vero cells (Fig. 7a), suggesting its unlikely for DZNep to induce drug-resistant viral variants.

In absence of any drug, P40-Control and P40-DZNep viruses replicated with similar viral titers (Fig. 7a), although, as compared to P0, they replicated at significantly higher titers (~8-fold) (Fig. 7a). In addition, as compared to the P0 virus, P40-Control and P40-DZNep viruses also produced bigger size plaques (Fig. 7b). This could have occurred due to long-term propagation of the virus in the cell culture which led to acquisition of some non-specific mutations (irrespective of the drug treatment) that enabled them to replicate more efficiently.

3.8. In ovo antiviral efficacy of DZNep against virulent infection of IBV

In order to evaluate the *in vitro* to *in vivo* translational potential of DZNep, IBV egg infection model was employed as described previously (Kumar et al., 2021). Non-lethal dose(s) (Fig. 8a) of DZNep prevented the death of chicken embryos against virulent IBV challenge in a dose-dependent manner (Fig. 8b). Besides, DZNep treatment also resulted in the normal development of embryos, as compared to control embryos wherein stunted growth and defective feather development was observed (Fig. 8c).

4. Discussion

The rapidly emerging field of epitranscriptomics has mapped several modifications in mRNA and their impact on gene expression. Only 2–5% of cellular RNA is mRNA (Anreiter et al., 2021). Further, the abundance of mRNA modifications is low, with a prevalence rate of <0.5% of all nucleotides (Dong et al., 2016; Xu et al., 2017). These modifications are variable in the range of 5–88% at a given site or transcript (Liu et al., 2013; Molinie et al., 2016). m6A is the most predominant epitranscriptomic modification in mRNA, accounting for 0.1–0.5% of all adenosines (Kadumuri and Janga, 2018). Despite an extremely low distribution, they play important roles in cellular homeostasis (Shi et al., 2019; Xu et al., 2017) and are dysregulated in several disease conditions including viral infections (Brocard et al., 2017; Manners et al., 2019; Mauer and Jaffrey, 2018). SARS-CoV-2 infection also triggers a global increase in m6A methylome (Liu et al., 2021). The levels of m6A methylome in our study varied from 0.02 to 0.09% (Fig. 3b), depending on the course of virus infection. Since cell free SARS-CoV-2 particles do not harbour any significant m6A modifications (<0.003%) (Fig. 3b), these are deposited inside the host cell and removed before formation and budding of the mature virion particles. However, some viruses can maintain a relatively high amount of m6A-modified genome in the intact virion particles (Choy et al., 2020), suggesting a complex pattern of epitranscriptomic regulation of virus replication.

To gain a detailed view on the impact of methylation on virus replication, we treated the cells with a sub-cytotoxic concentration of DZNep (methyl transferase inhibitor) and examined its effect on the

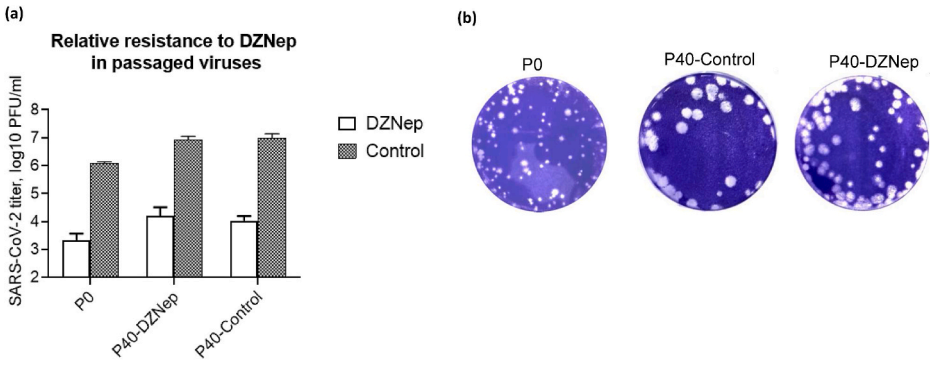

Fig. 7. Selection of DZNep-resistant SARS-CoV-2 mutants. Vero cells were infected with SARS-CoV-2 at MOI of 0.01 and grown in the presence of either 0.5 μg/ml of DZNep or vehicle control (0.05% DMSO). The progeny virus particles released in the supernatant was harvested either at 48–72 hpi or when ~75% cells exhibited CPE. Forty (40) such sequential passages were made. Thereafter, Vero cells, in triplicate, were infected with P0, P40-DZNep or P40-Control passaged viruses (SARS-CoV-2) at MOI of 0.1 in the presence of either 1 μg/ml of DZNep or 0.05% DMSO and the progeny virus particles released in the supernatant at 24 hpi were quantified by plaque assay **(a).**Values are means ± SD and representative of the result of at least 3 independent experiments. Plaque morphology of P0, P40-Control and P40-DZNep viruses is also shown **(b).**

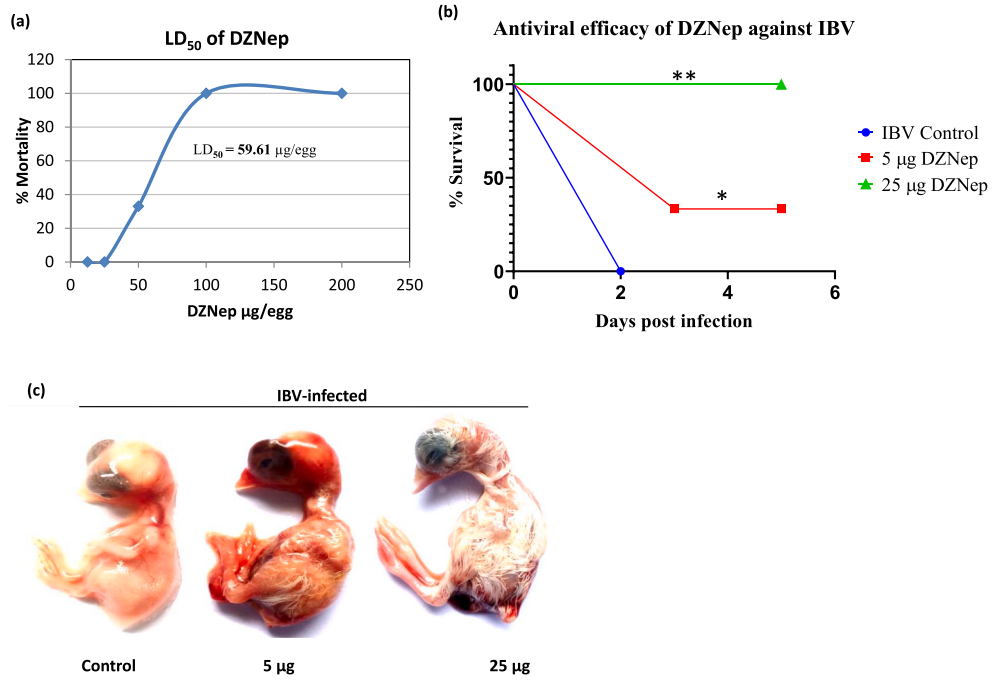

Fig. 8. In ovo antiviral efficacy of DZNep against IBV: SPF embryonated chicken eggs, in triplicates, were infected with IBV at EID_{50} of 100 via allantoic route in the presence of indicated concentrations of DZNep or equivalent volume of DMSO and observed daily for mortality of the embryos. LD_{50} was determined by the Reed-Muench method **(a).** Duration of the survival of chicken embryos following IBV challenge as determined by Kaplan-Meier (survival) curve is shown **(b).** Statistical analysis in survival curves was made using Log-rank (Mantel-Cox) Test using GraphPad Prism 8.0 software. Morphological changes in the chicken embryos at different drug regimens following IBV challenge is also shown (c). * = $P < 0.05$, ** = $P < 0.01$.

individual steps of SARS-CoV-2 replication. DZNep decreased the levels of viral genome and protein synthesis, without affecting other steps of the viral life cycle such as attachment, entry and budding. The participation of m6A machinery in synthesizing SARS-CoV-2 genome was further confirmed by a reduced immunoprecipitation of SARS-CoV-2 RNA by α-m6A in DZNep treated cells in a CHIP assay.

Next we identified the reader of m6A modification for SARS-CoV-2 RNA. *In silico* binding studies, immunoprecipitation of SARS-CoV-2 RNA by α-hnRNPA1, together with lower levels of RNA immunoprecipitation in the DZNep treated cells confirmed that hnRNPA1serves as an m6A reader and facilitates synthesis of SARS-CoV-2 RNA. Since DZNep did not directly affect the level of hnRNPA1 expression, its inhibitory effect is mediated via RNA-protein interaction rather than by reduced hnRNPA1 expression.

Besides low levels of viral RNA, DZNep treatment also resulted in a decreased synthesis of SARS-CoV-2 proteins. This could be a reflection of low levels of mRNA or direct interruption in protein synthesis. In coronaviruses, viral mRNA translation takes place in a cap-dependent manner (Stukalov et al., 2021) wherein the eIF4E plays a central role in the initiation of translation (Kumar et al., 2021). Upon activation by upstream kinase(s), elF4E binds to the 5′ cap of mRNA to initiate translation (Kumar et al., 2018b, 2021). The 5′-cap structure of viral mRNA also undergoes at least two epitranscriptomic (methylation) modifications viz; m7G and cOMe (Imam et al., 2020; Liu et al., 2021). Reduced immunoprecipitation of SARS-CoV-2 mRNA by α-peIF4E from DZNep-treated cells suggested that methylation (m7G and cOMe) of the 5′ cap of viral mRNA is essential for its interaction with eIF4E-a prerequisite for translation of viral proteins (Kumar et al., 2021). Alternatively, reduced levels of viral proteins in the DZNep-treated cells could also be due to defective synthesis of the 5′ cap of viral mRNA. In a cell-free viral mRNA and cellular p-eIF4E interaction assay, perturbation of the epitranscriptomic machinery by DZNep resulted in the production of viral RNA which was not able to interact properly with eIF4E, suggesting that methylation of the cap-adjacent nucleotides of SARS-CoV-2 mRNA is essential for the proper formation of the 5′ cap.

Immediately following infection, the nascent positive sense viral RNA is directly translated to produce a polyprotein. The polyprotein is further cleaved to produce 16 non-structural proteins (NSPs), which then facilitates the transcription of genomic and subgenomic RNAs (Finkel et al., 2021; Stukalov et al., 2021). We reveal that this early switch from translation to replication in the viral life cycle is regulated by epitranscriptomic modifications. Initially we observed a switch

on/off phenomenon in the hnRNPA1 expression levels in SARS-CoV-2 infected Vero cells (Fig. 4a). This, together with previous studies on m6A-mediated repression of cellular translation (Slobodin et al., 2017), tempted us to speculate that hnRNPA1 could be involved in switching from translation to replication of SARS-CoV-2 RNA. It has been hypothesized that besides viral proteins, RBPs also play an important role in switching from translation to replication of the viral genome (Gamarnik and Andino, 1998, 2000; Li and Nagy, 2011), although there is very limited experimental proof (Gamarnik and Andino, 2000). Recruitment of cellular factors associated with translation (p-eIF4E) at 1 hpi and those associated with transcription (methylome/hNRNPA1) at 2 hpi indicated the involvement of epitranscriptomic marks in switching from translation to transcription. Perturbation of m6A pathway (2 hpi) resulted in a defective hnRNPA1-mediated synthesis of SARS-CoV-2 RNA which further confirmed the recruitment of epitranscriptomic machinery during viral transcription (Fig. 6b). Furthermore, we also demonstrated (at 2 hpi) that hnRNPA1 (but not eIF4E) interacts with m6A-marked internal RNA and inhibition of m6A modification results in an arrest in hnRNPA1-mediated synthesis of SARS-CoV-2 genome (Fig. 6c and d). These lines of evidence clearly suggest that installation of m6A marks in the SARS-CoV-2 RNA recruit hnRNPA1 that eventually facilitates transcription and represses translation (Fig. 9), a novel role of epitranscriptomic machinery in regulating switch from translation to replication in SARS-CoV-2 life cycle.

Depending on the nature of the virus replication, depletion of the m6A machinery may have differential pro-(Courtney et al., 2017; Kennedy et al., 2017; Lichinchi et al., 2016a; Tirumuru et al., 2016) or anti-viral (Gokhale et al., 2016; Lichinchi et al., 2016b) impact on viral life cycle (Hesser et al., 2018). Methyltransferase inhibitor DZNep together with siRNA knockdown of METTL3 (m6A writer), hNRNPA1 (m6A reader) and MAT2A (enzyme that participates in the synthesis of SAM-the universal methyl donor) in Vero cells resulted in a reduced virus yield indicating that the m6A epitranscriptomic machinery facilitates SARS-CoV-2 replication and could serve as a novel target for antiviral drug development. These findings are in agreement with other two recent studies which have demonstrated virus supportive function of METTL3 (Burgess et al., 2021; Li et al., 2021). Contrary, in another study, Liu et al. (2021), revealed a negative impact of m6A methylome on SARS-CoV-2 gene expression. However, this study by Liu et al. was based on measuring "S" protein expression as an indicator of virus infection, rather than quantifying virus yield employed in ours and two other studies (Hesser et al., 2018; Tan et al., 2018). Nevertheless, our study suggests that methylation may differentially regulate transcription and translation of SARS-CoV-2 genome, depending on the course of virus replication.

The requirement of the cellular factors is usually conserved among multiple strains of a particular virus or even across multiple members of a given virus family (Chander et al., 2021; Khandelwal et al., 2020; Kumar et al., 2011a, 2011b, 2019). We demonstrated *in vitro* antiviral efficacy of DZNep (inhibitor that targets cellular factor-methyl transferase) against both wild-type and Delta strains of SARS-CoV-2, besides demonstrating it's protective effect against lethal IBV (*Coronaviridae* family member) infection in embryonated chicken eggs suggesting a broad-spectrum antiviral effect.

Antiviral drug resistance is a matter of great clinical importance. The inherent ability of the RNA viruses to rapidly acquire drug-resistance is a major challenge in developing antiviral drugs (Kumar et al., 2016). Most of the direct virus-acting agents rapidly induce drug-resistant phenotypes (Kumar et al., 2011b, 2020). Inhibitor such as DZNep (epidrug) blocks SARS-CoV-2 replication by targeting a cellular factor (m6A pathway), therefore the emergence of drug-resistant viral mutants would seem to be unlikely as has been observed with other host-directed antiviral agents (Chaudhary et al., 2015; Kumar et al., 2008, 2011a, 2018a, 2018b, 2019, 2020; Xu et al., 2020). Because of its low tendency in generating drug-resistant viral variants, DZNep might possibly be useful as a salvage therapy in clinical settings where the virus has developed resistance to other available drugs. However, since such drugs would also inhibit the epitranscriptomic modification of cellular mRNAs, they may lead to toxicity (Kumar et al., 2020) and should be preferably used for treating the acute infections. Nevertheless, the majority of the host-directed agents which are in clinical use against cardiovascular and inflammatory diseases or cancers have minimal or no adverse side effects (Zeisel et al., 2013).

The effectiveness of the epigenetic machinery may depend on the environment (Karagiannis and Maulik, 2012; Metere and Graves, 2020), microbiota (Sharma et al., 2019), nutrition (Greco et al., 2019) and comorbidities (Jakovljevic and Borovecki, 2018), implying that a given viral RNA genome may perform differently in different individuals. In this context, our study which highlights the impact of an epitranscriptomic layer of regulation on the life cycle of SARS-CoV-2 is likely to contribute in understanding the pathogenicity, transmission and disease severity in the COVID-19 patients.

To conclude, we report that methylation of SARS-CoV-2 RNA regulates translation to replication switch in viral life cycle. Inhibiting this RNA modification pathway by chemical inhibitors (DZNep) may provide significant therapeutic effect against SARS-CoV-2 and other

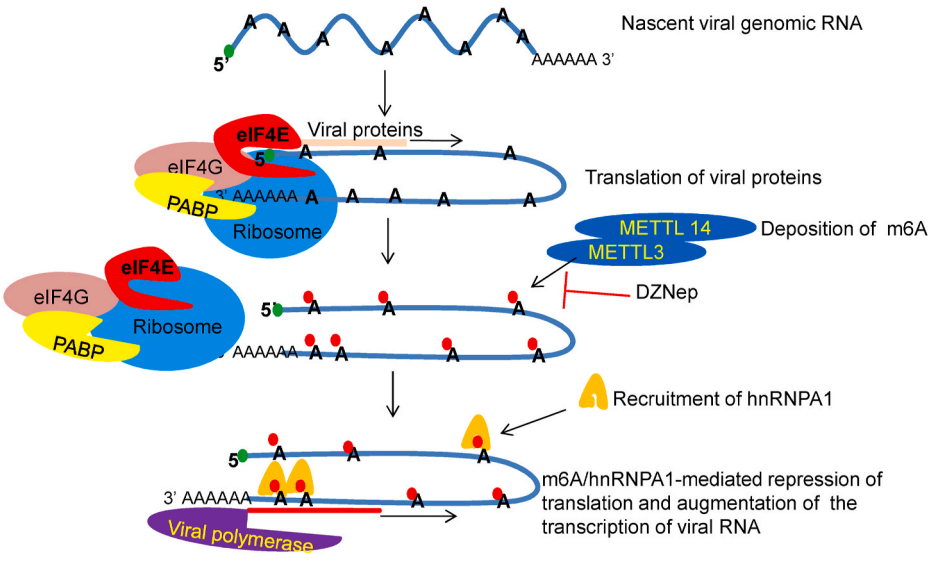

Fig. 9. Role of epitranscriptomic machinery in SARS-CoV-2 replication. Immediately following infection (~1h), the nascent positive sense SARS-CoV-2 RNA interacts with cap-dependent translational initiation machinery to directly translate the viral polyprotein which is further cleaved to produce 16 NSPs. After sometime (~2h), viral RNA is subjected to m6A modifications (eight m6A sites in SARs-CoV-2 genome) via cellular writers such as METTL3 and METTL14. m6A deposition facilitates recruitment of hnRNPA1 (three hnRNPA1 binding sites-two at 3′ end and one in "S" gene) which eventually repress translation and facilitate transcription-switch of viral RNA from translation to transcription. DZNep treatment inhibits deposition of m6A mark on SARS-CoV-2 RNA which eventually inhibits recruitment of hnRNPA1 and hence reduces synthesis of the viral RNA.

coronaviruses, without generating any drug-resistant viral variants.

Declaration of competing interest

The authors declare that they have no known competing financial interests or personal relationships that could have appeared to influence the work reported in this paper.

Acknowledgements

This work was supported by Indian Council of Agricultural Research, New Delhi (grant number IXX14586 to N-Ku and NASF/ABA-8027/2020-21 to N-Ku and B.R.G.) and Science and Engineering Research Board, Department of Science and Technology, Government of India (grant number CVD/2020/000103 to N-Ku). The funders had no role in study design, data collection and analysis, decision to publish, or preparation of the manuscript. A preprint of this manuscript is available at bioRxiv preprint repository (https://doi.org/10.1101/2021.07.13.452288).

Appendix A. Supplementary data

Supplementary data to this article can be found online at https://doi.org/10.1016/j.antiviral.2021.105232.

References

Anreiter, I., Mir, Q., Simpson, J.T., Janga, S.C., Soller, M., 2021. New twists in detecting mRNA modification dynamics. Trends Biotechnol. 39, 72–89.
Beig Parikhani, A., Bazaz, M., Bamehr, H., Fereshteh, S., Amiri, S., Salehi-Vaziri, M., Arashkia, A., Azadmanesh, K., 2021. The inclusive review on SARS-CoV-2 biology, epidemiology, diagnosis, and potential management options. Curr. Microbiol. 78, 1099–1114.
Boccaletto, P., Baginski, B., 2021. MODOMICS: an operational guide to the use of the RNA modification pathways database. Methods Mol. Biol. 2284, 481–505.
Brocard, M., Ruggieri, A., Locker, N., 2017. m6A RNA methylation, a new hallmark in virus-host interactions. J. Gen. Virol. 98, 2207–2214.
Burgess, H.M., Depledge, D.P., Thompson, L., Srinivas, K.P., Grande, R.C., Vink, E.I., Abebe, J.S., Blackaby, W.P., Hendrick, A., Albertella, M.R., Kouzarides, T., Stapleford, K.A., Wilson, A.C., Mohr, I., 2021. Targeting the m(6)A RNA modification pathway blocks SARS-CoV-2 and HCoV-OC43 replication. Genes Dev. 35, 1005–1019.
Chander, Y., Kumar, R., Khandelwal, N., Singh, N., Shringi, B.N., Barua, S., Kumar, N., 2021. Role of p38 mitogen-activated protein kinase signalling in virus replication and potential for developing broad spectrum antiviral drugs. Rev. Med. Virol. 31, 1–16.
Chaudhary, K., Chaubey, K.K., Singh, S.V., Kumar, N., 2015. Receptor tyrosine kinase signaling regulates replication of the peste des petits ruminants virus. Acta Virol. 59, 78–83.
Choi, Y.H., Hagedorn, C.H., 2003. Purifying mRNAs with a high-affinity eIF4E mutant identifies the short 3′ poly (A) end phenotype. Proc. Natl. Acad. Sci. Unit. States Am. 100, 7033–7038.
Chokkalla, A.K., Mehta, S.L., Vemuganti, R., 2020. Epitranscriptomic regulation by m(6)A RNA methylation in brain development and diseases. J. Cerebr. Blood Flow Metabol. 40, 2331–2349.
Choy, K.T., Wong, A.Y., Kaewpreedee, P., Sia, S.F., Chen, D., Hui, K.P.Y., Chu, D.K.W., Chan, M.C.W., Cheung, P.P., Huang, X., Peiris, M., Yen, H.L., 2020. Remdesivir, lopinavir, emetine, and homoharringtonine inhibit SARS-CoV-2 replication in vitro. Antivir. Res. 178, 104786.
Courtney, D.G., Kennedy, E.M., Dumm, R.E., Bogerd, H.P., Tsai, K., Heaton, N.S., Cullen, B.R., 2017. Epitranscriptomic enhancement of influenza A virus gene expression and replication. Cell Host Microbe 22, 377–386 e375.
Daffis, S., Szretter, K.J., Schriewer, J., Li, J., Youn, S., Errett, J., Lin, T.Y., Schneller, S., Zust, R., Dong, H., Thiel, V., Sen, G.C., Fensterl, V., Klimstra, W.B., Pierson, T.C., Buller, R.M., Gale Jr., M., Shi, P.Y., Diamond, M.S., 2010. 2′-O methylation of the viral mRNA cap evades host restriction by IFIT family members. Nature 468, 452–456.
Dominissini, D., Moshitch-Moshkovitz, S., Schwartz, S., Salmon-Divon, M., Ungar, L., Osenberg, S., Cesarkas, K., Jacob-Hirsch, J., Amariglio, N., Kupiec, M., Sorek, R., Rechavi, G., 2012. Topology of the human and mouse m6A RNA methylomes revealed by m6A-seq. Nature 485, 201–206.
Dong, C., Niu, L., Song, W., Xiong, X., Zhang, X., Zhang, Z., Yang, Y., Yi, F., Zhan, J., Zhang, H., Yang, Z., Zhang, L.H., Zhai, S., Li, H., Ye, M., Du, Q., 2016. tRNA modification profiles of the fast-proliferating cancer cells. Biochem. Biophys. Res. Commun. 476, 340–345.
Finkel, Y., Gluck, A., Nachshon, A., Winkler, R., Fisher, T., Rozman, B., Mizrahi, O., Lubelsky, Y., Zuckerman, B., Slobodin, B., Yahalom-Ronen, Y., Tamir, H., Ulitsky, I., Israely, T., Paran, N., Schwartz, M., Stern-Ginossar, N., 2021. SARS-CoV-2 uses a multipronged strategy to impede host protein synthesis. Nature 594, 240–245.
Galloway, A., Cowling, V.H., 2019. mRNA cap regulation in mammalian cell function and fate. Biochim Biophys Acta Gene Regul Mech 1862, 270–279.
Gamarnik, A.V., Andino, R., 1998. Switch from translation to RNA replication in a positive-stranded RNA virus. Genes Dev. 12, 2293–2304.
Gamarnik, A.V., Andino, R., 2000. Interactions of viral protein 3CD and poly(rC) binding protein with the 5' untranslated region of the poliovirus genome. J. Virol. 74, 2219–2226.
Gokhale, N.S., McIntyre, A.B.R., McFadden, M.J., Roder, A.E., Kennedy, E.M., Gandara, J.A., Hopcraft, S.E., Quicke, K.M., Vazquez, C., Willer, J., Ilkayeva, O.R., Law, B.A., Holley, C.L., Garcia-Blanco, M.A., Evans, M.J., Suthar, M.S., Bradrick, S. S., Mason, C.E., Horner, S.M., 2016. N6-Methyladenosine in flaviviridae viral RNA genomes regulates infection. Cell Host Microbe 20, 654–665.
Greco, E.A., Lenzi, A., Migliaccio, S., Gessani, S., 2019. Epigenetic modifications induced by nutrients in early life phases: gender differences in metabolic alteration in adulthood. Front. Genet. 10, 795.
Hesser, C.R., Karijolich, J., Dominissini, D., He, C., Glaunsinger, B.A., 2018. N6-methyladenosine modification and the YTHDF2 reader protein play cell type specific roles in lytic viral gene expression during Kaposi's sarcoma-associated herpesvirus infection. PLoS Pathog. 14, e1006995.
Imam, H., Kim, G.W., Siddiqui, A., 2020. Epitranscriptomic(N6-methyladenosine) modification of viral RNA and virus-host interactions. Front Cell Infect Microbiol 10, 584283.
Jakovljevic, M., Borovecki, F., 2018. Epigenetics, resilience, comorbidity and treatment outcome. Psychiatr. Danub. 30, 242–253.
Kadumuri, R.V., Janga, S.C., 2018. Epitranscriptomic code and its alterations in human disease. Trends Mol. Med. 24, 886–903.
Karagiannis, T.C., Maulik, N., 2012. Factors influencing epigenetic mechanisms and related diseases. Antioxidants Redox Signal. 17, 192–194.
Kennedy, E.M., Bogerd, H.P., Kornepati, A.V.R., Kang, D., Ghoshal, D., Marshall, J.B., Poling, B.C., Tsai, K., Gokhale, N.S., Horner, S.M., Cullen, B.R., 2017. Posttranscriptional m(6)A editing of HIV-1 mRNAs enhances viral gene expression. Cell Host Microbe 22, 830.
Khandelwal, N., Chander, Y., Kumar, R., Riyesh, T., Dedar, R.K., Kumar, M., Gulati, B.R., Sharma, S., Tripathi, B.N., Barua, S., Kumar, N., 2020. Antiviral activity of Apigenin against buffalopox: novel mechanistic insights and drug-resistance considerations. Antivir. Res. 181, 104870.
Khandelwal, N., Chander, Y., Rawat, K.D., Riyesh, T., Nishanth, C., Sharma, S., Jindal, N., Tripathi, B.N., Barua, S., Kumar, N., 2017. Emetine inhibits replication of RNA and DNA viruses without generating drug-resistant virus variants. Antivir. Res. 144, 196–204.
Kumar, N., Barua, S., Thachamvally, R., Tripathi, B.N., 2016. Systems perspective of morbillivirus replication. J. Mol. Microbiol. Biotechnol. 26, 389–400.
Kumar, N., Khandelwal, N., Kumar, R., Chander, Y., Rawat, K.D., Chaubey, K.K., Sharma, S., Singh, S.V., Riyesh, T., Tripathi, B.N., Barua, S., 2019. Inhibitor of sarco/endoplasmic reticulum calcium-ATPase impairs multiple steps of paramyxovirus replication. Front. Microbiol. 10, 209.
Kumar, N., Liang, Y., Parslow, T.G., Liang, Y., 2011a. Receptor tyrosine kinase inhibitors block multiple steps of influenza a virus replication. J. Virol. 85, 2818–2827.
Kumar, N., Sharma, N.R., Ly, H., Parslow, T.G., Liang, Y., 2011b. Receptor tyrosine kinase inhibitors that block replication of influenza a and other viruses. Antimicrob. Agents Chemother. 55, 5553–5559.
Kumar, N., Sharma, S., Kumar, R., Tripathi, B.N., Barua, S., Ly, H., Rouse, B.T., 2020. Host-directed antiviral therapy. Clin. Microbiol. Rev. 33.
Kumar, N., Xin, Z.T., Liang, Y., Ly, H., Liang, Y., 2008. NF-kappaB signaling differentially regulates influenza virus RNA synthesis. J. Virol. 82, 9880–9889.
Kumar, R., Afsar, M., Khandelwal, N., Chander, Y., Riyesh, T., Dedar, R.K., Gulati, B.R., Pal, Y., Barua, S., Tripathi, B.N., Hussain, T., Kumar, N., 2021. Emetine suppresses SARS-CoV-2 replication by inhibiting interaction of viral mRNA with eIF4E. Antivir. Res. 189, 105056.
Kumar, R., Khandelwal, N., Chander, Y., Riyesh, T., Tripathi, B.N., Kashyap, S.K., Barua, S., Maherchandani, S., Kumar, N., 2018a. MNK1 inhibitor as an antiviral agent suppresses buffalopox virus protein synthesis. Antivir. Res. 160, 126–136.
Kumar, R., Khandelwal, N., Thachamvally, R., Tripathi, B.N., Barua, S., Kashyap, S.K., Maherchandani, S., Kumar, N., 2018b. Role of MAPK/MNK1 signaling in virus replication. Virus Res. 253, 48–61.
Li, N., Hui, H., Bray, B., Gonzalez, G.M., Zeller, M., Anderson, K.G., Knight, R., Smith, D., Wang, Y., Carlin, A.F., Rana, T.M., 2021. METTL3 regulates viral m6A RNA modification and host cell innate immune responses during SARS-CoV-2 infection. Cell Rep. 35, 109091.
Li, Z., Nagy, P.D., 2011. Diverse roles of host RNA binding proteins in RNA virus replication. RNA Biol. 8, 305–315.
Lichinchi, G., Gao, S., Saletore, Y., Gonzalez, G.M., Bansal, V., Wang, Y., Mason, C.E., Rana, T.M., 2016a. Dynamics of the human and viral m(6)A RNA methylomes during HIV-1 infection of T cells. Nat Microbiol 1, 16011.
Lichinchi, G., Zhao, B.S., Wu, Y., Lu, Z., Qin, Y., He, C., Rana, T.M., 2016b. Dynamics of human and viral RNA methylation during zika virus infection. Cell Host Microbe 20, 666–673.
Liu, J., Xu, Y.P., Li, K., Ye, Q., Zhou, H.Y., Sun, H., Li, X., Yu, L., Deng, Y.Q., Li, R.T., Cheng, M.L., He, B., Zhou, J., Li, X.F., Wu, A., Yi, C., Qin, C.F., 2021. The m(6)A methylome of SARS-CoV-2 in host cells. Cell Res. 31 (4), 404–414.
Liu, N., Parisien, M., Dai, Q., Zheng, G., He, C., Pan, T., 2013. Probing N6-methyladenosine RNA modification status at single nucleotide resolution in mRNA and long noncoding RNA. RNA 19, 1848–1856.

Manners, O., Baquero-Perez, B., Whitehouse, A., 2019. m(6)A: widespread regulatory control in virus replication. Biochim Biophys Acta Gene Regul Mech 1862, 370–381.
Masse, M., Glippa, V., Saad, H., Le Bloas, R., Gauffeny, I., Berthou, C., Czjzek, M., Cormier, P., Cosson, B., 2014. An eIF4E-interacting peptide induces cell death in cancer cell lines. Cell Death Dis. 5 e1500-e1500.
Mauer, J., Jaffrey, S.R., 2018. FTO, m(6) Am , and the hypothesis of reversible epitranscriptomic mRNA modifications. FEBS Lett. 592, 2012–2022.
McHugh, C.A., Chen, C.-K., Chow, A., Surka, C.F., Tran, C., McDonel, P., Pandya-Jones, A., Blanco, M., Burghard, C., Moradian, A., 2015. The Xist lncRNA interacts directly with SHARP to silence transcription through HDAC3. Nature 521, 232–236.
Metere, A., Graves, C.E., 2020. Factors influencing epigenetic mechanisms: is there A role for bariatric surgery? High Throughput 9 (1), 6.
Meyer, K.D., Saletore, Y., Zumbo, P., Elemento, O., Mason, C.E., Jaffrey, S.R., 2012. Comprehensive analysis of mRNA methylation reveals enrichment in 3' UTRs and near stop codons. Cell 149, 1635–1646.
Molinie, B., Wang, J., Lim, K.S., Hillebrand, R., Lu, Z.X., Van Wittenberghe, N., Howard, B.D., Daneshvar, K., Mullen, A.C., Dedon, P., Xing, Y., Giallourakis, C.C., 2016. m(6)A-LAIC-seq reveals the census and complexity of the m(6)A epitranscriptome. Nat. Methods 13, 692–698.
Ramanathan, M., Porter, D.F., Khavari, P.A., 2019. Methods to study RNA–protein interactions. Nat. Methods 16, 225–234.
Schwartz, D.C., Parker, R., 2000. mRNA decapping in yeast requires dissociation of the cap binding protein, eukaryotic translation initiation factor 4E. Mol. Cell Biol. 20, 7933–7942.
Seo, K.W., Kleiner, R.E., 2021. Mechanisms of epitranscriptomic gene regulation. Biopolymers 112, e23403.
Sharma, M., Li, Y., Stoll, M.L., Tollefsbol, T.O., 2019. The epigenetic connection between the gut microbiome in obesity and diabetes. Front. Genet. 10, 1329.
Shi, H., Wei, J., He, C., 2019. Where, when, and how: context-dependent functions of RNA methylation writers, readers, and erasers. Mol. Cell. 74, 640–650.
Slobodin, B., Han, R., Calderone, V., Vrielink, J.A.O., Loayza-Puch, F., Elkon, R., Agami, R., 2017. Transcription impacts the efficiency of mRNA translation via co-transcriptional N6-adenosine methylation. Cell 169, 326–337.
Stukalov, A., Girault, V., Grass, V., Karayel, O., Bergant, V., Urban, C., Haas, D.A., Huang, Y., Oubraham, L., Wang, A., Hamad, M.S., Piras, A., Hansen, F.M., Tanzer, M. C., Paron, I., Zinzula, L., Engleitner, T., Reinecke, M., Lavacca, T.M., Ehmann, R., Wolfel, R., Jores, J., Kuster, B., Protzer, U., Rad, R., Ziebuhr, J., Thiel, V., Scaturro, P., Mann, M., Pichlmair, A., 2021. Multilevel proteomics reveals host perturbations by SARS-CoV-2 and SARS-CoV. Nature 594, 246–252.
Suzuki, K., Bose, P., Leong-Quong, R.Y., Fujita, D.J., Riabowol, K., 2010. REAP: a two minute cell fractionation method. BMC Res. Notes 3, 1–6.
Tan, B., Liu, H., Zhang, S., da Silva, S.R., Zhang, L., Meng, J., Cui, X., Yuan, H., Sorel, O., Zhang, S.W., Huang, Y., Gao, S.J., 2018. Viral and cellular N(6)-methyladenosine and N(6),2'-O-dimethyladenosine epitranscriptomes in the KSHV life cycle. Nat Microbiol 3, 108–120.
Tirumuru, N., Zhao, B.S., Lu, W., Lu, Z., He, C., Wu, L., 2016. N(6)-methyladenosine of HIV-1 RNA regulates viral infection and HIV-1 Gag protein expression. Elife 5.
Trotman, J.B., Giltmier, A.J., Mukherjee, C., Schoenberg, D.R., 2017. RNA guanine-7 methyltransferase catalyzes the methylation of cytoplasmically recapped RNAs. Nucleic Acids Res. 45, 10726–10739.
Xu, L., Liu, X., Sheng, N., Oo, K.S., Liang, J., Chionh, Y.H., Xu, J., Ye, F., Gao, Y.G., Dedon, P.C., Fu, X.Y., 2017. Three distinct 3-methylcytidine (m(3)C) methyltransferases modify tRNA and mRNA in mice and humans. J. Biol. Chem. 292, 14695–14703.
Xu, X., Miao, J., Shao, Q., Gao, Y., Hong, L., 2020. Apigenin suppresses influenza A virus-induced RIG-I activation and viral replication. J. Med. Virol. 92 (12), 3057–3066.
Zeisel, M.B., Lupberger, J., Fofana, I., Baumert, T.F., 2013. Host-targeting agents for prevention and treatment of chronic hepatitis C - perspectives and challenges. J. Hepatol. 58, 375–384.
Zhao, Y., Shi, Y., Shen, H., Xie, W., 2020. m(6)A-binding proteins: the emerging crucial performers in epigenetics. J. Hematol. Oncol. 13, 35.